Classification of Ambiguous Nerve Fiber Orientations in 3D Polarized Light Imaging

Melanie Kleiner[1], Markus Axer[1,2], David Gräßel[1], Julia Reckfort[1],
Uwe Pietrzyk[1,2], Katrin Amunts[1,3], and Timo Dickscheid[1]

[1] Institute of Neuroscience and Medicine (INM-1, INM-4),
Research Center Jülich,Germany
[2] Department of Physics, University of Wuppertal, Germany
[3] Department of Psychiatry, Psychotherapy and Psychosomatics,
RWTH Aachen University, Germany

Abstract. 3D Polarized Light Imaging (3D-PLI) has been shown to measure the orientation of nerve fibers in post mortem human brains at ultra high resolution. The 3D orientation in each voxel is obtained as a pair of angles, the direction angle and the inclination angle with unknown sign. The sign ambiguity is a major problem for the correct interpretation of fiber orientation. Measurements from a tiltable specimen stage, that are highly sensitive to noise, extract information, which allows drawing conclusions about the true inclination sign. In order to reduce noise, we propose a global classification of the inclination sign, which combines measurements with spatial coherence constraints. The problem is formulated as a second order Markov random field and solved efficiently with graph cuts. We evaluate our approach on synthetic and human brain data. The results of global optimization are compared to independent pixel classification with subsequent edge-preserving smoothing.

1 Introduction

Fiber tracts are composed of axons, which connect nerve cells between each other, and thus transmit information between brain areas. The exact courses of fiber tracts are still far from being fully understood. Several methods for mapping fiber tracts have been developed to approach a complete model of all fiber tracts, the *connectome*. 3D-PLI is a method that measures the birefringence of lipids surrounding single axons (myelin sheath) by transmitting polarized light through histological sections [1], [2]. 3D fiber orientations can be reconstructed at micro scale resolution (Fig. 1(a)). For comparison, the measurement of water diffusion by Diffusion Weighted Magnetic Resonance Imaging (DW-MRI) can resolve fiber orientations in vivo [3], but on scales of millimeters.

In 3D-PLI measurements, the sign of the fiber inclination angle is unknown. This ambiguity has been addressed previously by Larsen et al. [4], who used a simulated annealing technique to optimize a smoothness criterion, but did not collect additional measurements about the inclination sign at each individual pixel. Pajdzik et al. [5] developed a microscope tilting-stage to identify the sign

of the optical indicatrix of birefringent, uniaxial crystals, which corresponds to the inclination sign in the context of 3D-PLI.

The inclination sign ambiguity can be regarded as a binary labeling problem, similar to segmentation or denoising in digital imaging, that can be solved efficiently by Markov random field (MRF) theory [6], [7].

2   3D Polarized Light Imaging

Polarimeter Setup. Linearly polarized light is transmitted through a brain section, a retarder, an analyzer and then imaged by a digital camera (Fig. 1(b)). The polarizing filters are rotated simultaneously to generate a series of intensity images. The measured signal can be modeled as a sine curve with phase φ and amplitude r [8]. Referring to the histological sectioning plane, the parameter φ (*direction*) corresponds to the in-plane angle of measured fibers in relation to the polarizing filters. The parameter r (*retardation*) is correlated nonlinearly with the out-of-plane angle α (*inclination*). The pair of angles (φ, α) represents a 3D

(a)   (b)
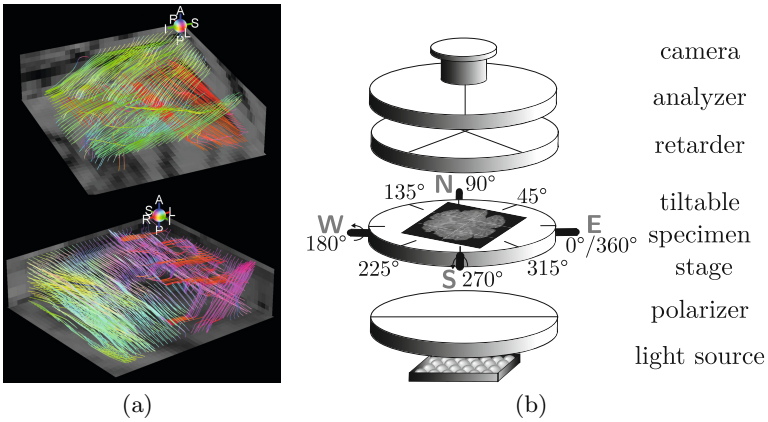
Fig. 1. (a) Reconstructed fiber tracts from 3D-PLI as presented in [2, Fig. 6] (b) The 3D-PLI setup shows a specimen stage, which is tiltable in four directions (N, W, E, S). The measured in-plane fiber direction φ is related to the polarizing filters and annotated in degrees. The inclination sign can be derived most reliably, when the tilting direction and the in-plane fiber direction are similar.

fiber orientation with unknown direction. To avoid alternating notations for the same orientation, we restrict φ to $[0°, 180°]$ and α to $[-90°, 90°]$. According to [8, Eq. 6], α can be approximated as

$$|\alpha| = \arccos\left(\sqrt{\frac{2 \cdot \arcsin(r)}{\pi \cdot d_{\text{rel}}}}\right) \tag{1}$$

with a reference value d_{rel} depending on section thickness, wavelength and birefringence. Assuming a constant value of d_{rel} ignores the inhomogeneity of the examined tissue, and limits the accuracy of (1). The restriction to slice thicknesses with $d_{\mathrm{rel}} \leq 1$ is necessary for a bijective relation between $|\alpha|$ and r. Equation (1) shows that only the absolute value of α can be determined from r, which leads to the *inclination sign ambiguity* in 3D-PLI.

Tilting Setup. In addition to the measurement of the flat specimen stage, further measurements can be acquired in four tilting directions $\psi \in \{\mathrm{north(N)}=90°,$ $\mathrm{west(W)}=180°, \mathrm{east(E)}=0°, \mathrm{south(S)}=270°\}$ by tilting the stage along one of two perpendicular axes. All tilted images are registered to the flat image by a projective linear transformation. The specimen stage is tilted by the angle $\tau \leq 4°$ to avoid strong distortions. The relation between tilting directions and fiber in-plane directions is illustrated in Fig. 1(b). We denote the tilted measurements by α^ψ and r^ψ in contrast to α and r on a flat specimen stage. For each tilting direction ψ, the *opposite* direction is $\psi \pm 180°$. If the fiber in-plane direction and the tilting direction are similar, fibers with positive inclination can be distinguished from those with negative inclination by their decrease in absolute inclination after tilting (Fig. 2(a)). Otherwise, the change is less significant or even inversed. Generally, these changes are marginal and hence very sensitive to noise. We can formalize this relationship for fiber directions $\varphi \in (\psi - 90°, \psi + 90°)$ as

$$\alpha \geq 0 \Leftrightarrow |\alpha^\psi| \leq |\alpha^{\psi\pm180°}| \,. \tag{2}$$

(a)   (b)
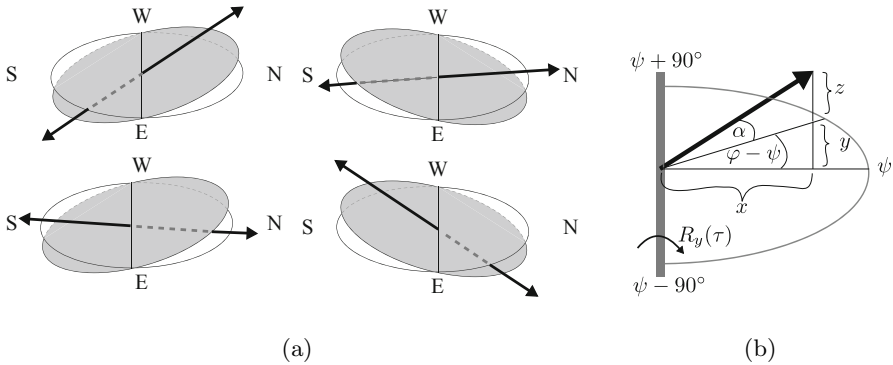
Fig. 2. (a) The absolute inclination, i. e. steepness, of fibers with a positive inclination sign (top row) decreases when tilting from S to N. If the inclination sign is negative (bottom row), the steepness increases. (b) The fiber orientation can be represented as a vector $\boldsymbol{v} = (x, y, z)^{\mathrm{T}}$. A tilt by the angle τ can be modeled as a rotation $R_y(\tau)$ applied to $\boldsymbol{v}$.

3   Solving the Inclination Sign Ambiguity

The classification of the inclination sign can be considered as a labeling problem. Given the image domain Ω and a binary set of labels $\mathcal{S} = \{-1, +1\}$ reflecting the unknown inclination sign, we want to find a *labeling function* $s : \Omega \to \mathcal{S}$ that assigns one of two possible values to every $i \in \Omega$. A second order MRF can take spatial coherence into account and leads to an energy function of the form

$$E(s) = \sum_i \theta_i(s_i) + \lambda \cdot \sum_{(i,j) \in \mathcal{N}} \theta_{i,j}(s_i, s_j) \, . \tag{3}$$

for any non-negative potentials θ_i (*data potential*), $\theta_{i,j}$ (*smoothness potential*) and a neighborhood relation $\mathcal{N}$.

Data Potential. A large difference between oppositely tilted, unsigned inclination angles $|\alpha^\psi| - |\alpha^{\psi \pm 180°}|$ indicates high reliability of a positive inferred inclination sign. We therefore require the data potential to be proportional to the sum of these differences for all tilting directions, i. e.

$$\theta_i \propto \sum_\psi |\alpha_i^\psi| - |\alpha_i^{\psi \pm 180°}| \, . \tag{4}$$

However, due to the reference value d_{rel} in (1), the inclination values possess limited accuracy. Therefore, we develop an alternative formulation that does not require d_{rel}. We achieve this by deriving the sign and the absolute value of the given difference separately.

First, we take advantage of the dependency

$$|\alpha_i^\psi - \alpha_i^{\psi \pm 180°}| \approx 2 \cdot \cos(\varphi_i - \psi) \cdot \sin(\tau) \, , \tag{5}$$

which is restricted to small angles τ, such that $\tau \approx \sin(\tau)$. Equation (5) is obtained by rotating the flat fiber orientation vector as shown in Fig. 2(b). Second, we need the sign of $|\alpha_i^\psi| - |\alpha_i^{\psi \pm 180°}|$ to distinguish positive and negative inclination signs. Again, we avoid the approximation of inclination angles by (1). Instead, we consider the difference of retardation values $r_i^\psi - r_i^{\psi \pm 180°}$. The non-linear relation between inclination α_i and retardation r_i, is strictly decreasing (for $d_{\mathrm{rel}} \leq 1$, see (1)), so we expect

$$\mathrm{sgn}(\alpha_i^\psi - \alpha_i^{\psi \pm 180°}) = \mathrm{sgn}(r_i^{\psi \pm 180°} - r_i^\psi) \, . \tag{6}$$

Equations (6) and (5) finally lead to the data potential

$$\theta_i \propto \sum_\psi \cos(\varphi_i - \psi) \cdot \sin(\tau) \cdot \mathrm{sgn}(r_i^{\psi \pm 180°} - r_i^\psi) \tag{7}$$

that does not require d_{rel}. By inserting $\psi \in \{\text{E}=0°, \text{N}=90°, \text{W}=180°, \text{S}=270°\}$, and applying a normalization term, (7) becomes

$$\theta_i(s_i) = \frac{1}{2} + s_i \cdot \frac{\sin(\varphi_i) \cdot \mathrm{sgn}(r_i^N - r_i^S) + \cos(\varphi_i) \cdot \mathrm{sgn}(r_i^E - r_i^W)}{2\sqrt{2}} \, . \tag{8}$$

Smoothness Potential. We assume that neighboring pixels tend to belong to the same anatomical structure with a similar fiber orientation. Hence, if neighboring pixels have similar in-plane fiber directions, their inclination signs are very likely to be the same as well. This leads to a *contrast-sensitive Potts model* [9, Eq. 3], where the contrast is defined as the absolute difference of neighboring in-plane angles.

$$\theta_{i,j}(s_i, s_j) = \left(1 - \frac{|\varphi_i - \varphi_j|}{180°}\right) \cdot \begin{cases} 1 & \text{, if } s_i \neq s_j \\ 0 & \text{, else} \end{cases} \tag{9}$$
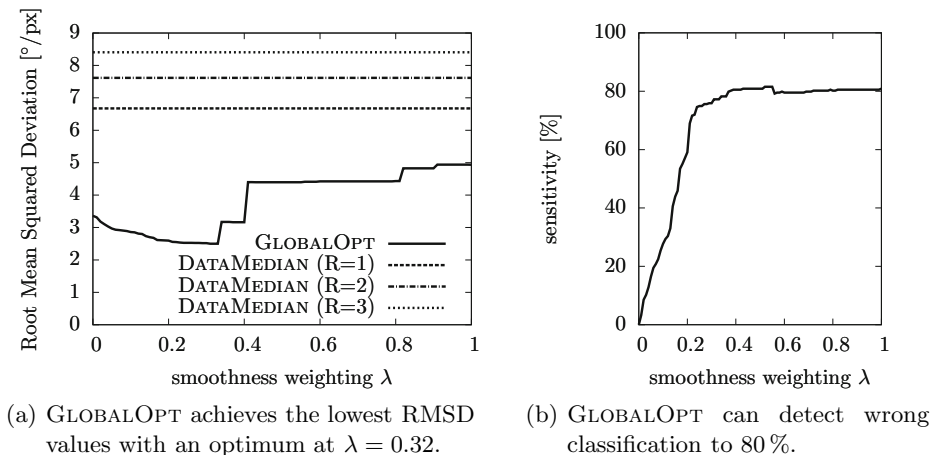
This function is regular and graph-representable according to [7, Theorem 4.1]. Therefore, the minimization of (3) can be computed efficiently via graph cuts.

4   Evaluation

The inclination sign and the resulting vector fields are evaluated on synthetic images and selected regions of various human brain sections. The presented approach by MRF optimization (GLOBALOPT) is compared to the direct determination of the inclination sign by tilted measurements (DATAONLY), which corresponds to GLOBALOPT without a smoothness potential ($\lambda = 0$). The third approach to be compared is DATAONLY with subsequent median filtering with variable radius (DATAMEDIAN).

Synthetic Data. A synthetic data set consisting of a direction image $\tilde{\varphi}$ and an inclination image $\tilde{\alpha}$ was created. The structure consists of rounded and crossing fiber tracts (Fig. 4(a)). The corresponding direction measurements φ were simulated by adding noise with $\sigma_\varphi = 0.5$. The retardation measurements r were simulated in several steps. First, the tilted inclination angles $\tilde{\alpha}^\psi$ were calculated by rotation as shown in Fig. 2(b). Second, retardation values were calculated from $\tilde{\alpha}$ according to (1) with $d_{\text{rel}} = 0.4$. Finally, noise was added with $\sigma_r = 0.006$. The simulated inclination measurements α were obtained from the absolute inclination $|\alpha|$ calculated from r and an inclination sign $s \in \{s^\lambda, s^R \text{ or } s'\}$. s^λ was determined by GLOBALOPT and weighting factor λ, s' was determined by DATAONLY, and s^R was determined by DATAMEDIAN with radius $R \in \{1, 2, 3\}$. The noise levels σ_r and σ_φ were determined in 30 repeated measurements.

For evaluation, the true orientation vector $\tilde{\boldsymbol{v}}$ was composed from the synthetic orientation angles $\tilde{\varphi}$ and $\tilde{\alpha}$. Accordingly, the orientation vector $\boldsymbol{v} \in \{\boldsymbol{v}^\lambda, \boldsymbol{v}^R, \boldsymbol{v}'\}$ was composed from the simulated measurements φ and α. The difference between the true and the simulated vector field was measured by the root mean squared deviation (RMSD) of both vectors at each pixel location. Background pixels displayed in black in Fig. 4(a) are not considered. Fig. 3(a) shows that GLOBALOPT achieves an RMSD of 2.5° (optimum at $\lambda = 0.32$) compared to DATAONLY with an RMSD of 3.36° and DATAMEDIAN with RMSD values above 6°. The sensitivity of GLOBALOPT to determine the correct inclination sign at pixels that are not classified correctly by DATAONLY was examined in Fig. 3(b).

(a) GLOBALOPT achieves the lowest RMSD values with an optimum at $\lambda = 0.32$.

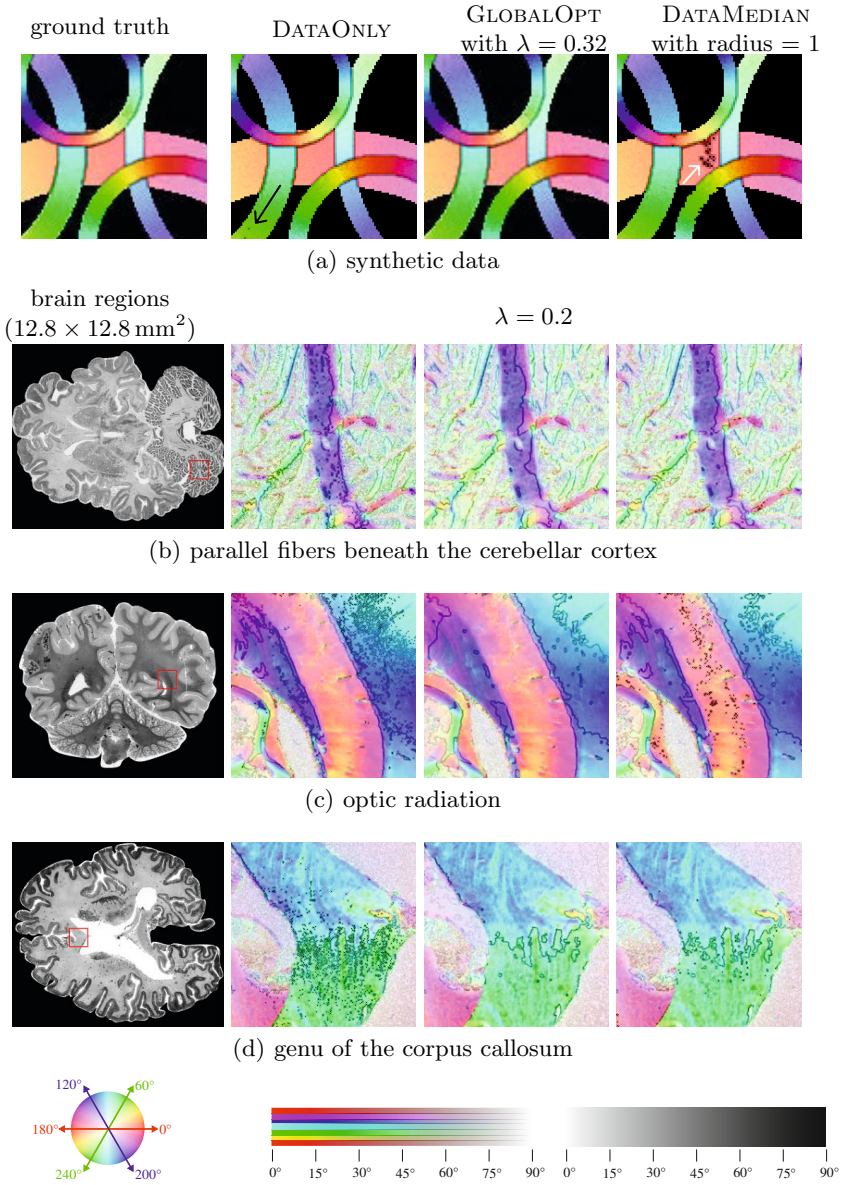(b) GLOBALOPT can detect wrong classification to 80 %.

Fig. 3. evaluation of the determined inclination signs on synthetic data

Human Brain Data. Regions in histological sections of three post mortem brains without pathological findings were selected to demonstrate the different behavior of all approaches (Fig. 4(b)–(d)). The manual evaluation of inclination signs requires an appropriate visualization of the vector field. The resulting 3D orientations were visualized in HSV color space, but brightness was reduced where local differences were high in terms of the mean absolute deviation (MAD) in the local 8-neighborbood of each pixel i. The color coding (Fig. 4(e)) emphasizes abrupt changes in a vector field by dark pixels or edges. Accordingly, unexpected changes in the vector fields, which could be caused by wrong inclination signs, are made visible. For GLOBALOPT, the results appeared best with $\lambda = 0.2$. This is not equal to the optimum for synthetic data ($\lambda = 0.32$), which reflects the lack of realistic noise modeling in the simulation.

Both GLOBALOPT and DATAMEDIAN are able to remove isolated deviating inclination signs in DATAONLY, which is shown in the white matter beneath the cerebellar cortex, containing mainly parallel fibers (Fig. 4(b)). DATAMEDIAN introduces severe artifacts into the vector field, which is demonstrated in the optic radiation (Fig. 4(c)). The inhomogeneous vector field in the corpus callosum (Fig. 4(d)), where fibers of both hemispheres cross to the contralateral side, also clearly benefits from regularization. GLOBALOPT with $\lambda = 0.2$ and DATAMEDIAN with $R = 1$ eliminate noise on an equal level, while GLOBALOPT with $\lambda = 0.32$ slightly oversmoothes the vector field. The influence of λ is strong and therefore must be determined carefully.

5   Discussion

The classification of ambiguous inclination signs is an essential step, when determining the fiber orientation in 3D-PLI. Until now, the inclination sign ambiguity

(a) synthetic data

(b) parallel fibers beneath the cerebellar cortex

(c) optic radiation

(d) genu of the corpus callosum

$\mathrm{Hue}(\varphi) = 2\varphi$ $\mathrm{Saturation}(\alpha) = |\alpha|/90°$ $\mathrm{Value}(\mathrm{MAD}) = 1 - \mathrm{MAD}$

(e) HSV color coding. The mean absolute deviation (MAD) of each vector to its neighbors was emphasized as decreased brightness to visualize the homogeneity of the resulting vector fields.

Fig. 4. On brain data, the apparently best results were achieved with GLOBALOPT for $\lambda = 0.2$. The quantitative evaluation on synthetic images determined the optimum for GLOBALOPT at $\lambda = 0.32$. The parallel fibers beneath the cerebellar cortex and the corpus callosum demonstrate the benefit of regularization opposed to DATAONLY. The optic radiation shows that DATAMEDIAN introduces undesired artifacts.

has been tackled by using either tilted measurements [5] or context information [4] separately. We have presented a global solution for this problem based on a second order Markov random field, which considers both sources of information simultaneously. In contrast to DW-MRI, which aims at identifying fiber pathways with a millimeter resolution, 3D-PLI aims at ultra-high resolution up to a few microns. Working with such high spatial accuracy demands for eliminating as much noise as possible. In our experiments, the new method better conserves the true inclination sign than sole tilted measurements with subsequent edge-preserving smoothing by a median filter, which has shown to introduce artifacts. These problems especially appear where the fiber direction angle changes from $0°$ to $180°$ and vice versa. In contrast to the proposed contrast-sensitive smoothness term, the median sorting criterion cannot adequately handle these changes. The global optimization leaves a single parameter controlling the influence of context information. In the synthetic data set, $\lambda = 0.32$ is optimal, while $\lambda = 0.2$ seems optimal for real data. Future work will include further validation with reference tissue samples to enable more precise analysis of errors. With a well-balanced smoothness term, the presented method shows significant improvements, but only on a small fraction of pixels. However, considering the envisaged accuracy, we believe that such a small fraction is still crucial for meaningful fiber tracking.

References

1. Larsen, L., Griffin, L.D., Graessel, D., Witte, O.W., Axer, H.: Polarized light imaging of white matter architecture. Microsc. Res. Techniq. 70(10), 851–863 (2007)
2. Axer, M., Gräßel, D., Kleiner, M., Dammers, J., Dickscheid, T., Reckfort, J., Hütz, T., Eiben, B., Pietrzyk, U., Zilles, K., Amunts, K.: High-resolution fiber tract reconstruction in the human brain by means of three-dimensional polarized light imaging (3d-pli). Front. Neuroinform. 5 (2011)
3. Hagmann, P., Jonasson, L., Maeder, P., Thiran, J.P., Wedeen, V.J., Meuli, R.: Understanding diffusion mr imaging techniques: From scalar diffusion-weighted imaging to diffusion tensor imaging and beyond. Radiographics 26(suppl. 1), S205–S223 (2006)
4. Larsen, L., Griffin, L.: Can a Continuity Heuristic Be Used to Resolve the Inclination Ambiguity of Polarized Light Imaging? In: Sonka, M., Kakadiaris, I.A., Kybic, J. (eds.) CVAMIA/MMBIA 2004. LNCS, vol. 3117, pp. 365–375. Springer, Heidelberg (2004)
5. Pajdzik, L.A., Glazer, A.M.: Three-dimensional birefringence imaging with a microscope tilting-stage. i. uniaxial crystals. J. Appl. Crystallogr. 39(3), 326–337 (2006)
6. Chen, S.Y., Tong, H., Cattani, C.: Markov models for image labeling. Math. Probl. Eng., Article ID 814356, 18 pages (2012)
7. Kolmogorov, V., Zabih, R.: What energy functions can be minimized via graph cuts? IEEE TPAMI 26(2), 147–159 (2004)
8. Axer, M., Amunts, K., Gräßel, D., Palm, C., Dammers, J., Axer, H., Pietrzyk, U., Zilles, K.: A novel approach to the human connectome: Ultra-high resolution mapping of fiber tracts in the brain. NeuroImage 54(2), 1091–1101 (2011)
9. Boykov, Y.Y., Jolly, M.P.: Interactive graph cuts for optimal boundary & region segmentation of objects in n-d images. In: IEEE ICCV 2004 (2001)